Proceedings of ASME Turbo Expo 2011
GT2011
June 6-10, 2011, Vancouver, British Columbia, Canada

GT2011-46125

NUMERICAL STUDY ON FLOW AND HEAT TRANSFER CHARACTERISTICS OF SWIRL COOLING ON LEADING EDGE MODEL OF GAS TURBINE BLADE

Zhao LIU, Zhenping FENG*, Liming SONG

Institute of Turbomachinery, Xi'an Jiaotong University, Xi'an 710049, P.R.CHINA
Tel/Fax: +86-29-82665062, *E-mail: zpfeng@mail.xjtu.edu.cn

ABSTRACT

In this paper a numerical simulation is performed to predict the swirl cooling on internal leading edge cooling passage model. The relative performances of four kinds of turbulence models including the standard κ-ε model, the RNG κ-ε model, the standard κ-ω model and the SST κ-ω model in the simulation of the swirl flow by tangential inlet jets in a circular pipe are compared with available experimental data. The results show that SST κ-ω model is the best one based on simulation accuracy. Then the SST κ-ω model is adopted for the present simulation. A circular pipe with a single rectangular tangential inlet jet or with two rectangular tangential inlet jets is adopted to investigate the swirl cooling and its effectiveness. The influence of the Reynolds number and the inlet to wall temperature ratio are investigated. The results indicate that the heat transfer coefficient on the swirl chamber increases with the increase of Reynolds number, and increases with the decrease of the inlet to wall temperature ratio. The swirl pipe with two tangential inlets could get a heat transfer enhancement of about three times to that of the nonswirling pipe, while swirl pipe with one tangential inlet could get a heat transfer coefficient 38% higher than that of the nonswirling pipe.

NOMENCLATURE

b	width of inlet duct (m)
D	swirl pipe diameter (m)
d	height of inlet duct (m)
G_x	local axial flux of linear momentum (kg s^{-2})
G_θ	local axial flux of angular momentum (kg m s^{-2})
h	local heat transfer coefficient (W m^{-2} K^{-1}), $= q_w /(T_w - T_j)$
L	length (span) of swirl pipe (m)
L_1	length of the second inlet duct to the end of the swirl pipe (m)
L_2	length of inlet duct (m)
L_3	length of outlet duct (m)
Nu	Nusselt number based on swirl pipe diameter, $= hD / \lambda$
Nu_a	axially area weighted average Nu
Nu_c	circumferentially area weighted average Nu
Nu_∞	Nusselt number for fully developed nonswirling turbulent pipe flow
Pr	Prandtl number
p	static pressure (Pa)
p_a	average static pressure (Pa)
p_t	total pressure of the impinging jet (Pa)
q_w	wall heat flux (Wm^{-2})
r	any radius in the swirl pipe (m)
R	inside radius of the swirl pipe (m)
Re	Reynolds number based on swirl pipe diameter and mean axial velocity, $= \rho UD / \mu$
S	local swirl number
T_w	wall surface temperature (K)
T_j	impinging jet air temperature (K)
U	mean axial velocity (m s^{-1})
u	axial component of point helical velocity of the air stream in the swirl pipe (m s^{-1})

u_τ	shear velocity (m s^{-1})
V	velocity magnitude (m s^{-1})
v	tangential component of point helical velocity of the air stream in the swirl pipe (m s^{-1})
x	span wise coordinate, swirl chamber axial direction (m)
Y	transverse coordinates from wall (m)
y^+	non-dimensional distance, $= Yu_\tau / \nu$

Greek

β	angle in the swirl chamber (deg)
μ	dynamic viscosity of fluid (Kg m^{-1} s^{-1})
λ	thermal conductivity of fluid (W m^{-1} K^{-1})
ν	kinematic viscosity (m^2 s^{-1})
ρ	density of fluid (Kg m^{-3})

INTRODUCTION

As modern gas turbine's operating temperature is increased continually for the sake of increasing the efficiency and power, turbine's inlet temperature has been already far beyond the material acceptable level, which results in high heat loads on the turbine components. It is worth to mention that the leading edge area witness higher heat flow as it is scoured by high temperature inflows. A series of cooling technologies, such as impingement cooling, swirl cooling and film cooling, have been applied in turbine leading edge. Swirl flow commonly referred to as a vortical flow with an axial velocity component can be generated by a number of methods, including twisted tape inserts, coil wires, propellers, inlet guided vanes and tangential injection of the fluid. Some of these methods generate swirl continuously along the entire length of the test section; while the others are placed at the inlet with decay of swirl along the tube.

Several studies of turbulent flow field in decaying swirl flows have been reported in the literature. Kreith and Margolis [1], and Kreith and Sonju [2] proposed a heat transfer enhancement concept in which swirl was introduced in the flow. In their concept, part of the fluid enters axially while the remainder is injected tangentially at various locations along the tube axis. And they obtained a solution for the equation to predict the decay of swirl through pipe. The first experimental study in this area was carried out by Nissan and Bresan [3] in 1961. In their work, swirl flow was produced by tangentially injecting water into a tube through two ports placed diametrically opposite to each other. At low flow rate (Re≤5000), the flow was going forward throughout the tube axially. At higher flow rates, there was a flow reversal in the core of the tube. Under some circumstances, there was visual evidence of double reversal with water flowing forward near the wall and in the center and moving backwards in the intervening region. Blum and Oliver [4] conducted experiments with two kinds of gases, air and carbon dioxide, and reported the heat transfer enhancement of decaying swirl flow relative to an axial flow, measured the local heat transfer coefficients in an electrically heated tube with swirling flow. An initial swirl generator with four square slots was used to inject the gas tangentially into the tube. The heat transfer coefficients were derived from the tube wall temperature rise for the fluid. The directions of the flow were explored in the separate experiment. Migay and Golubev [5] carried out a theoretical analysis to predict the heat transfer coefficient based on the evaluation of the equivalent friction factors for free swirling flows. Results showed that the free swirling flow increases the heat transfer rate, and the theoretical results and the experimental data were in excellent agreement. Algifri et al. [6] proposed a procedure to compute the swirl intensity, the tangential and axial velocity distributions for the given inlet flow conditions. Kitoh [7] experimentally studied the confined swirl flow generated with guide vanes. Guo and Dhir [8] using water as test fluid studied the effects of injection induced swirl on single and two phase heat transfer. They found a six fold increase in the local single phase heat transfer coefficient. Dhir and Chang [9], and Chang and Dhir [10, 11] using air as test fluid experimentally investigated the heat transfer enhancement in a tube by tangential injection. An enhancement of 35 to 40 percent on a constant pumping power basis was obtained with tangential injection. They also found that the enhancement is strongly dependent on the ratio of tangential to axial momentum flux but is weakly dependent on Reynolds number, and obtained profiles for mean velocities in the axial and tangential directions as well as the Reynolds stresses. Then they conducted extensive investigations on the spiral multi-tangential jets at the inlet and summarized it in a comprehensive correlation in terms of the maximum and average axial velocity ratio, average turbulence intensity, and the swirl number. Kumar and Conover [12] experimentally studied the 3-D flow dynamics of a cylindrical cyclone with tangential inlet and tangential exit using flow visualization. Li and Tomita [13] studied the characteristics of swirling flow in a circular pipe, and the decay of swirl, the average dynamic, static pressure, total pressure and the wall pressure was investigated experimentally. Fitouri et al. [14] described a multi-position single slant hot wire probe technique for the study of a 3-D confined vortex flow, and they carried out the corresponding derivation of the three main velocity components and six Reynolds stresses. Chen et al. [15] investigated both experimentally and numerically the swirl flow induced by tangential inlets in a circular pipe, and found that the flow pattern was very sensitive to the initial swirl intensity. Gomez et al. [16] experimentally studied the hydrodynamics of the continuous liquid phase under swirling two-phase flow using LDV, and they analyzed the swirling flow field and developed cyclone and pipe swirling flow field prediction correlations. Gül [17] experimentally investigated the effect of swirl flow on the heat transfer in a tube. Their results confirmed that the use of tangentially injections leads to a higher heat transfer rate over the plain tube. Also the augmentation of heat transfer was found to be the function of the tangential to total flow momentum ratio and Reynolds number, and no pronounced effect of injector number and angle on heat transfer was observed. Guo et al. [18] numerically studied a compressible tangentially injected swirling flow in the nozzle of air jet spinning, and investigated the effects of the nozzle geometric parameters on both the flow and yarn properties.

The previous investigations of swirling flow were focused on heat exchanger application, and the application of swirl cooling has not been investigated until by Hay and West [19] in 1970th. They investigated the decaying swirl by varying a single tangential jet angle to the channel axis at the upstream end, and proposed a possible application to gas turbine airfoil cooling. They measured local heat transfer coefficients and the flow field in a pipe at moderate Reynolds number (10,000 to 50,000). The heat transfer augmentation was found to be a function of the local swirl number, and a correlation for heat transfer was presented. Their results showed an increase of up to eightfold in local heat transfer. Then Glezer et al. [20] and Moon et al. [21] introduced a configuration with lengthwise continuous tangential injection. It generates swirl motions continuously without any decay along the entire length of a channel and compared it to other techniques of gas turbine airfoil cooling. Their investigation indicated that the channel diameter to jet slot height was the most important geometric parameter, and the pressure loss coefficient across the tangential slot was independent of the slot Reynolds number for a given geometry. They also gave out a dimensionless correlation between Nusselt number and Reynolds number. Ligrani et al. [22] and Thambu et al. [23] performed a flow visualization study to examine the relation between the generation of Görtler vortices and the augmented heat transfer characteristics in the cooling passage. Hedlund et al. [24, 25, 26] experimentally studied the flow and heat transfer of the swirl chamber. They used the smoke injection for flow visualization to identify vortex structures, used a five hole pressure probe to obtain time averaged surveys of total pressure, static pressure and the three mean velocity components, used infrared thermometer in conjunction with thermocouples, energy balances, digital image processing, and in situ calibration procedures to resolve temperature distribution, and together investigated the effects of Reynolds number and inlet coolant to wall temperature ratio on the heat transfer and flow structure. Hwang and Cheng [27, 28] measured the detailed heat transfer coefficient on the target wall with an array of orthogonal impinging jets by using transient liquid crystal technique. The angle between the inclined jets and the duct axis varied from 30º to 75º. They examined the effects of jet Reynolds number, exit flow orientation, duct shape and jet spacing on the heat transfer and pressure drop characteristics in triangular ducts, and found that the flow exiting from both sides of the duct performed the best heat transfer on the target surface. Ling et al. [29] experimentally and numerically studied a circular cooling passage with tangential injection suitable for a blade leading edge. They used hot wire anemometry to measure the vortex flow field and used transient liquid crystal technique to measure the heat transfer coefficients.

From the foregoing discussion, concerning the flow and heat transfer of swirl cooling on the turbine blade leading edge, it is clear that no systematic computational study is available in the previous studies. When the cooling jets impinging on the curved surface of turbine leading edge, the tangential velocity is affected by the jets Reynolds number, jet nozzle number and the crossflow created by the upstream jets (spent air). Those factors and the arrangement of the jets are the main factors which influence the heat transfer on the leading edge. Therefore, the present work is conducted to investigate the swirl cooling on a circular pipe with a single rectangular tangential inlet or two rectangular tangential inlets by using numerical method. The effects of jet Reynolds number and inlet to wall temperature ratio on flow and heat transfer characteristics are investigated in detail. Two different flow Reynolds numbers 10,500 and 24,600 for geometry (a), and three different flow Reynolds numbers 5,414, 7,219, and 9,024 for geometry (b) are simulated. And four ratios of inlet to wall temperature 0.65, 0.75, 0.83, and 0.95 in the same Reynolds number for geometry (b) are studied.

PHYSICAL AND MATHEMATICAL MODEL

A three dimensional steady system of turbulent flow of a single rectangular tangential jet or two rectangular tangential jets impinging on a turbine leading edge model is performed in the present investigation.

Geometrical details

In this work, the physical models for present numerical study (Fig.1(a) and Fig.1(b)) are chosen according to the experimental geometry measured by Hay et al. [19] and Ling et al. [29]. Figure 1(a) shows the physical geometry and boundary conditions of the experimental geometry by Hay et al., and Figure 1(b) shows the physical geometry and boundary conditions of the experimental geometry by Ling et al. The geometrical dimensions of different jet configurations involved in this paper are indicated in Table 1.

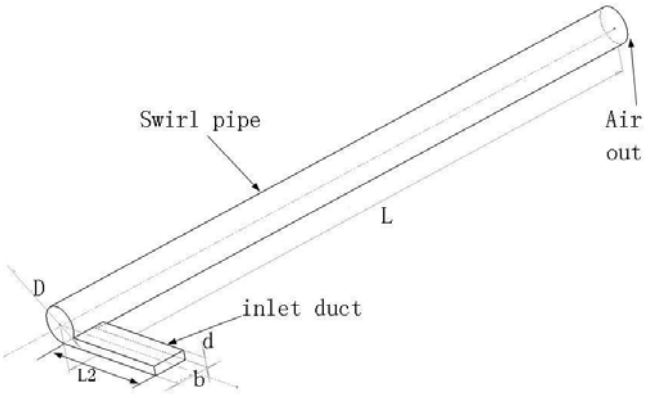

(a) Geometry measured by Hay et al. [19]

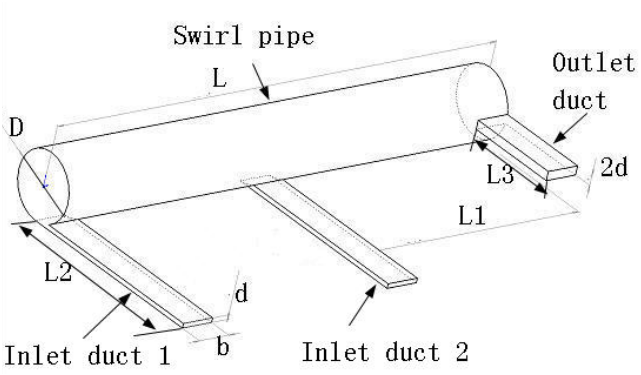

(b) Geometry measured by Ling et al. [29]

Fig. 1 Physical geometry and boundary conditions

Tab. 1 Geometric detail of jet configurations

	Geometry (a)	Geometry (b)
Dimension	Values	Values
D (mm)	50.8	70
L (mm)	914	525
L1 (mm)	-	245
L2 (mm)	175	210
L3 (mm)	-	135
Number of jets	1	2

Numerical method

The numerical simulations are performed by using a commercial CFD software CFX11.0. The solutions are obtained by solving the steady compressible Reynolds--averaged Navier-Stokes equations, in which a finite control volume method is applied to discretize these equations. The overall accuracy of the calculation is of the second order. Turbulence model is used to reflect the turbulent flow effect.

The software ICEMCFD is adopted to generate the unstructured grids for calculation regions. The mesh includes tetrahedral elements in the main flow passage, and prism elements in the near wall regions. In this study, there are two meshes for a particular geometry, one is for high Reynolds number κ-ε model and the other is for low Reynolds number κ-ω model. The wall grid y^+ is less than 1.0 when κ-ω model is used, and the wall grid y^+ is between 15 and 40 when κ-ε model is used, to reflect the turbulent flow effect. The ratio of cell size increases by about 30% outward from the walls in all cases. But the total grid nodes are almost the same for a particular geometry. The total grid nodes are about 1.7 million for geometry (a), and about 2.08 million for geometry (b). Figure 2 shows the grid generation result for geometry (a).

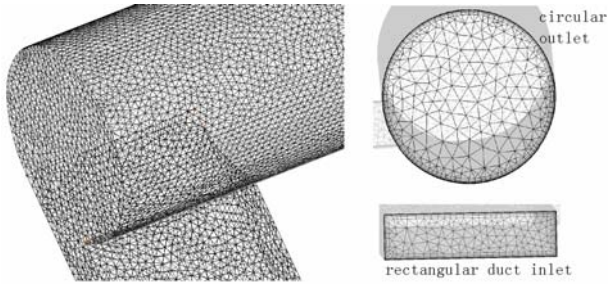

Fig. 2 Mesh in a pitch of the jet

The boundary conditions are matched with those in References [19] and [29]. As shown in Fig. 1, the rectangular cross sectioned inlet duct is considered as the inlet, the outlet is on the other end of the circular pipe in the experimental geometry by Hay et al., while the experimental geometry by Ling et al. has two rectangular inlet ducts and one rectangular outlet duct in the other end of the circular pipe. Mass flow and total temperature conditions are given at the inlet. Constant temperature is given at the pipe wall and average static pressure is given to the outlet. Inlet total temperature of geometry (a) is 348.15K, and inlet total temperature of geometry (b) is 239.85K. The inlet flow turbulent intensity for all the cases are in the range between 1% and 2%. The average static pressure at the outlets of the two geometries is 1atm. The fluid is air (ideal gas). The desired convergence target of each simulation is that the root mean square residuals of the momentum, mass equations, energy equation and turbulence equations are lower than 10^{-5} and remain steady.

TURBULENCE MODELS AND VALIDATION

In order to validate the ability of the different turbulence models to represent flow and heat transfer characteristics of the present work, two test cases are chosen. The first case investigated by Hay et al. [19] and the second case investigated by Ling et al. [29] are adopted as the model verification. The first case is with A_r=3.76, α =90°, *Re*=10,500 in Reference [19], and the second case is with *Re*=7,219 and T_j/T_w=0.83 in Reference [29].

Calculations are carried out with four turbulence models, the standard κ-ε model, the RNG κ-ε model, the standard κ-ω model and the SST κ-ω model, and the numerical results were compared with the available experimental data of Reference [19] and Reference [29].

Comparisons of the flow fields

The swirl number is defined as

$$S = \frac{G_\theta}{G_x R} = \frac{2\pi \int_0^R \rho r^2 uv dr}{2\pi R \int_0^R \rho r u^2 dr} \quad (1)$$

Figure 3 shows the comparison between the predicted and the available measured results by Hay et al. [19] involving the swirl number along the pipe. It is indicated that the swirl number of a single rectangular slot jet into the circular pipe couldn't be well simulated by any of the four turbulence models along the whole swirl chamber. There is a large calculation error at the inlet region and at the region from middle to outlet of the swirl chamber, but in the region just behind the inlet, the four turbulence models show very good simulation accuracy.

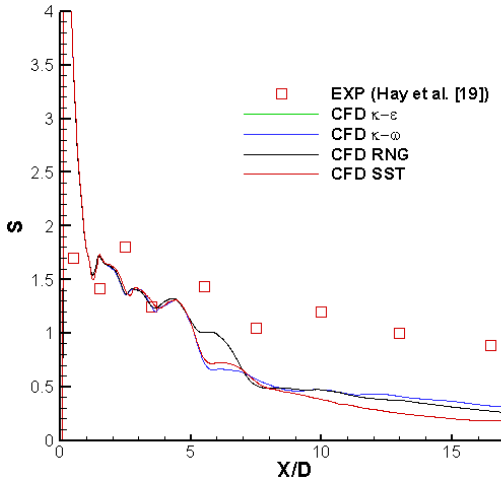

Fig. 3 Comparison of the swirl number predicted by different turbulence models in the swirl pipe with experimental results by Hay et al. [19]

The case with *Re*=7,219 and T_j/T_w=0.83 in Reference [29] was also adopted to validate the simulation accuracy of the four turbulence models. Figure 4 shows the comparison of the near wall velocity magnitude for angle β from 30° to 360° in

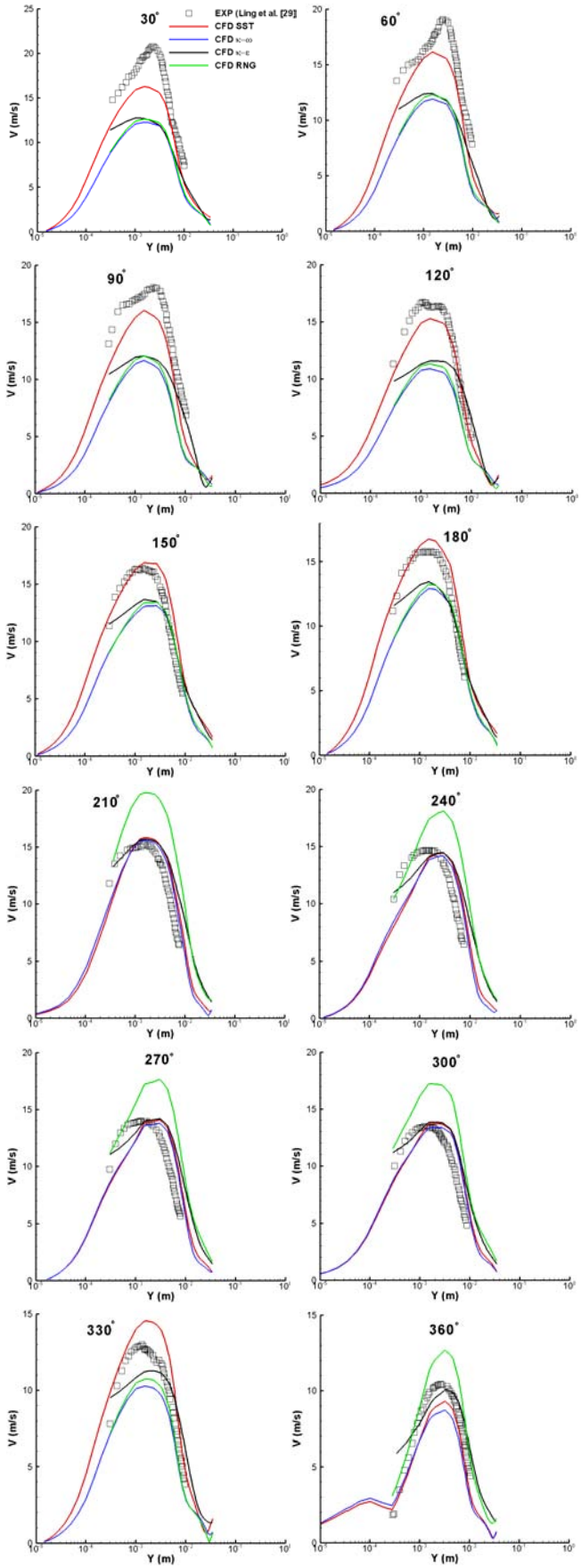

Fig. 4 Comparison of the near wall velocity magnitude predicted by different turbulence models with experimental results by Ling et al. [29] for β from 30° to 360° when x/R=0.5, Re=7219

the swirl pipe predicted by the four turbulence models with experimental results by Ling et al. [29] at x/R=0.5. The definition of angle β is shown in Fig.5. Figure 4 indicates that among the four turbulence models, the SST κ-ω model is the best one concerning the simulation accuracy and the variation trend of the simulation flow results, which is in good agreement with the experimental results.

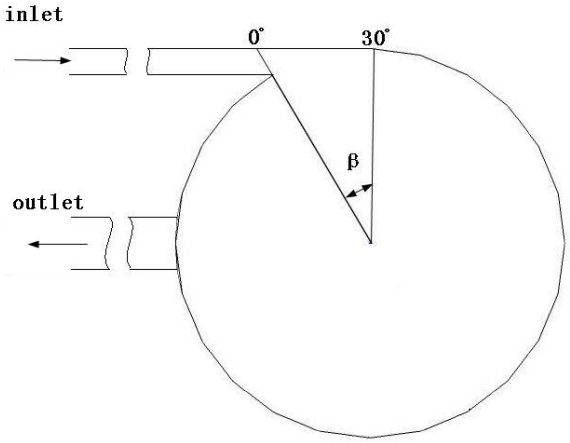

Fig. 5 Definition of angle β

Comparisons of the heat transfer

For a constant temperature surface, the local heat transfer coefficient can be expressed as

$$h = \frac{q_w}{T_w - T_j} \tag{2}$$

And the value of h can be normalized in the form of local Nusselt number as

$$Nu = \frac{hD}{\lambda} = \frac{q_w \cdot D}{(T_w - T_j)\lambda} \tag{3}$$

The values of Nu_∞ should be obtained from a relevant correlation for fully developed nonswirling turbulent flow. For example, the Dittus-Boelter equation is

$$Nu_\infty = 0.023\,\mathrm{Re}^{0.8}\,\mathrm{Pr}^n \tag{4}$$

where n is equal to 0.4 while heating the fluid, and 0.3 is adopted for cooling the fluid.

Figure 6 shows the comparison of relative circumferentially averaged Nusselt number predicted by the four turbulence models with experimental results by Hay et al. [19]. It is indicated that except the RNG κ-ε turbulence model, all other three turbulence models predicted results that agreed well with the experimental results in the region just behind the inlet, but in a large discrepancy from the middle to the outlet of the swirl chamber. This is in agreement with the swirl number shown in Fig. 3.

Figure 7 shows the comparison of local surface Nusselt number predicted by the three turbulence models with experimental results by Ling et al. [29] along β=210°. Because of the large error predicted by the standard κ-ε model, the result predicted by this model is not shown in Fig.7. As shown in Fig.4 and Fig.6, the results predicted by the RNG κ-ε model don't agree well with the experimental results. While for the standard κ-ω model and the SST κ-ω model, the predicted results agree well with the experimental results

along the swirl chamber at β=210°. And the SST κ-ω model is the best one concerning the simulation accuracy and the variation trend of the simulation results.

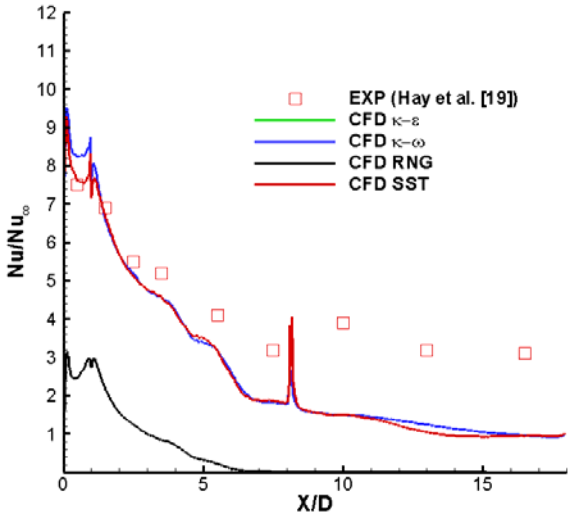

Fig. 6 Comparison of relative circumferentially averaged Nussselt number in the swirl pipe predicted by different turbulence models with experimental results by Hay et al. [19]

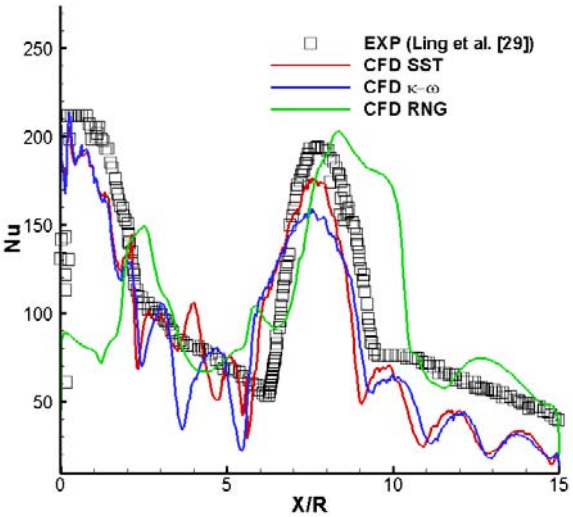

Fig. 7 Comparison of local surface Nussselt number by different turbulence models with experimental results by Ling et al. [29] along β=210°, Re=7219

Figure 8 shows the comparison of local surface Nusselt number predicted by the four turbulence models with experimental results by Ling et al. [29] at x/R=0.5, Re=7,219. It indicates that the results predicted by the standard κ-ε model and the RNG κ-ε model don't agree well with the experimental results. While for the standard κ-ω model and the SST κ-ω model, the predicted results agree well with the experimental results along the circumference of the swirl chamber at x/R=0.5 except at the near inlet region, and this is agreed with the velocity magnitude predicted by the four turbulence models shown in Fig.4.

Figure 9 shows the comparison of axially averaged Nusselt number variation with angle from inlet predicted by the four turbulence models with experimental results by Ling et al. [29]. It is also indicated that the results predicted by the standard κ-ω model and the SST κ-ω model agree well with the experimental results along the circumference of the swirl chamber, except for the abrupt increase in Nu_a in the region near 30°. The error in the range between 0° to 30° is that part of this area is in the inlet duct which is not take into account. The SST κ-ω model showed excellent simulation accuracy.

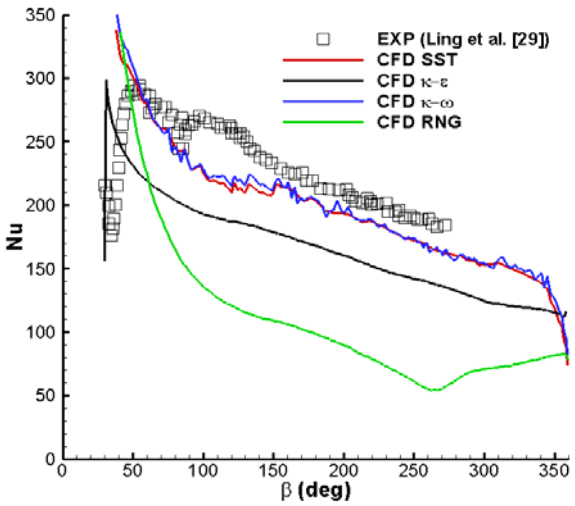

Fig. 8 Comparison of local surface Nussselt number by different turbulence models with experimental results by Ling et al. [29] at x/R=0.5, Re=7,219

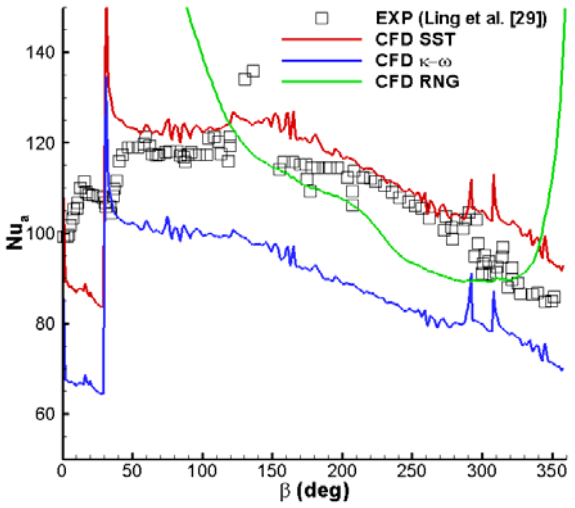

Fig. 9 Comparison of axially averaged Nussselt number variation with angle from inlet by different turbulence models with experimental results by Ling et al. [29]

Figure 10 shows the Comparison of circumferentially averaged Nussselt number along the axis of the swirl chamber by different turbulence models with experimental results by Ling et al. [29]. The SST κ-ω model presents excellent simulation accuracy on the Nu_c.

Based on the validation of the four turbulence models above, the SST κ-ω model is the best one concerning the simulation accuracy and the variation trend of the simulation results. All the following results reported are based on SST κ-ω model. All cases having the same geometry are investigated with the same domain grids and the same wall boundary conditions.

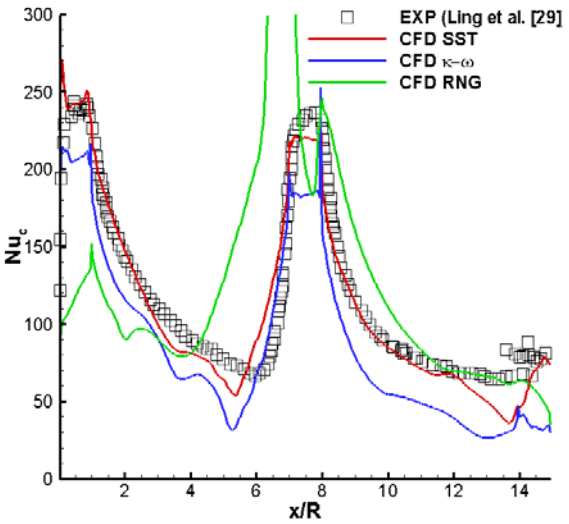

Fig. 10 Comparison of circumferentially averaged Nussselt number along the axis of the swirl chamber by different turbulence models with experimental results by Ling et al. [29]

RESULTS AND DISCUSSIONS

Effect of Reynolds number

Figure 11 shows the swirl number along the axis of the swirl chamber by different *Re* in geometry (a), and Fig. 12 shows the swirl number along the axis of the swirl chamber by different *Re* in geometry (b). It indicates that the swirl number isn't affected by the *Re* number, it only decay along the axis of the swirl chamber with the increase of *x/R*. The swirl number became to negative in the region near the second inlet duct in Fig. 12. This is because of the flow reversal led by the increase of the tangential velocity in this region.

Figure 13 shows the variation of relative pressure along the axis of the swirl chamber by different *Re* in geometry (b). The result also indicates that the relative pressure would barely change with the *Re* over the swirl chamber. The relative pressure increases along the axis of the swirl chamber and become lower in the second inlet.

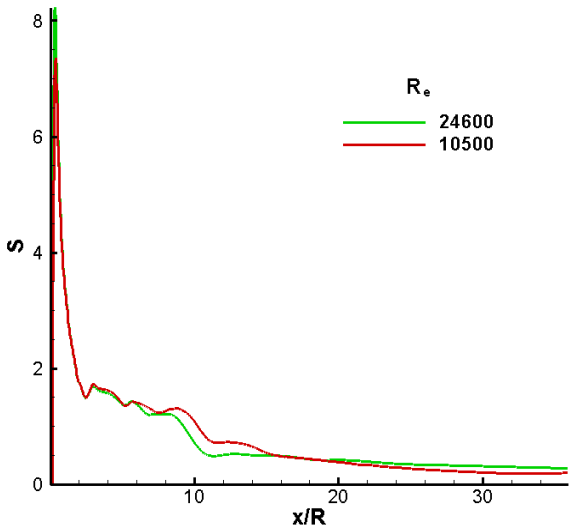

Fig. 11 The variation of swirl number along the axis of the swirl chamber with *Re* in geometry (a)

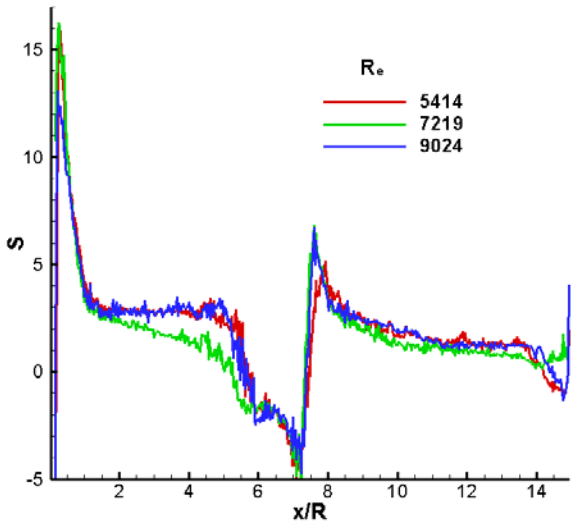

Fig. 12 The variation of swirl number along the axis of the swirl chamber with *Re* in geometry (b)

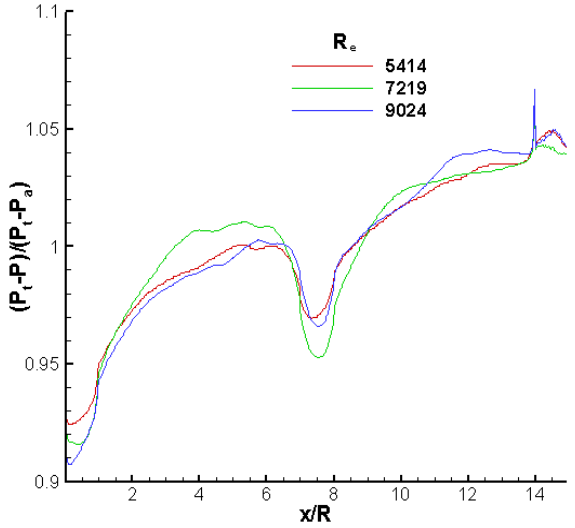

Fig. 13 The variation of relative pressure along the axis of the swirl chamber with *Re* in geometry (b)

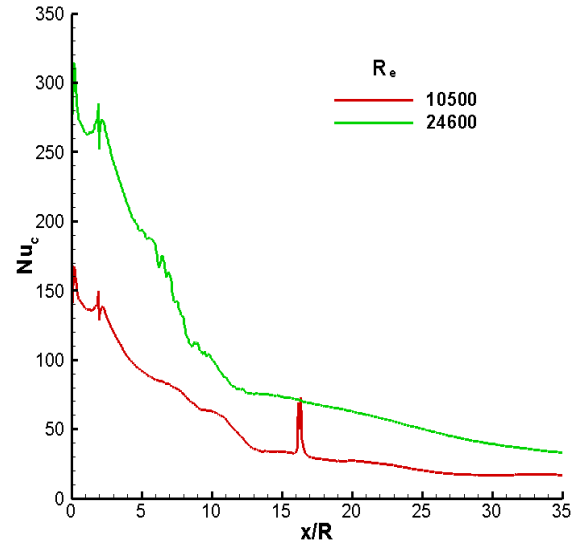

Fig. 14 The variation of circumferentially averaged Nusselt number along the axis of the swirl chamber with *Re* in geometry (a)

Figure 14 shows the variation of the area weighted circumferentially averaged Nusselt number along the axis of the swirl chamber by different *Re* in geometry (a). Figure 15 shows the variation of the area weighted circumferentially averaged Nusselt number along the axis of the swirl chamber by different *Re* in geometry (b). It is indicated that the Nu_c decays along the axial direction, and there is a distinct improvement in the region near the second tangential inlet. Because of the development of the new thermal boundary layer at each inlet, the development of the Görtler vortices, and the interactions between Görtler vortices and shear layer vortices, the peaks of Nu_c appear at the inlets. The convective activities are enhanced by the increase of *Re*, so the Nu_c increases with the increase of *Re* all along the axis of the swirl chamber. Figure 15 also shows good agreement of the numerical results with the experimental results by Ling et al. in the same condition.

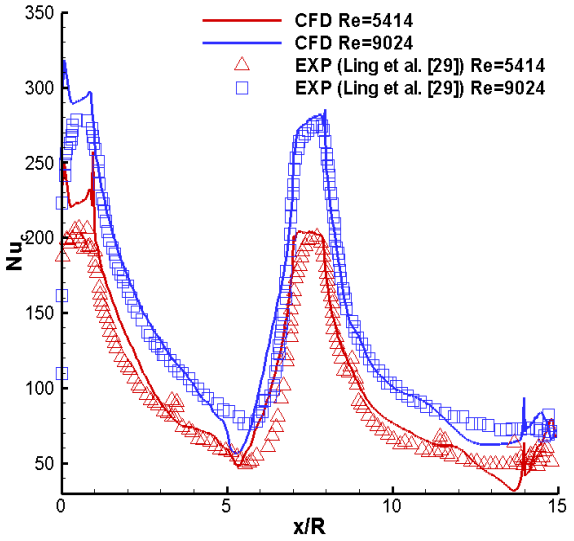

Fig. 15 The variation of circumferentially averaged Nussselt number along the axis of the swirl chamber with *Re* in geometry (b)

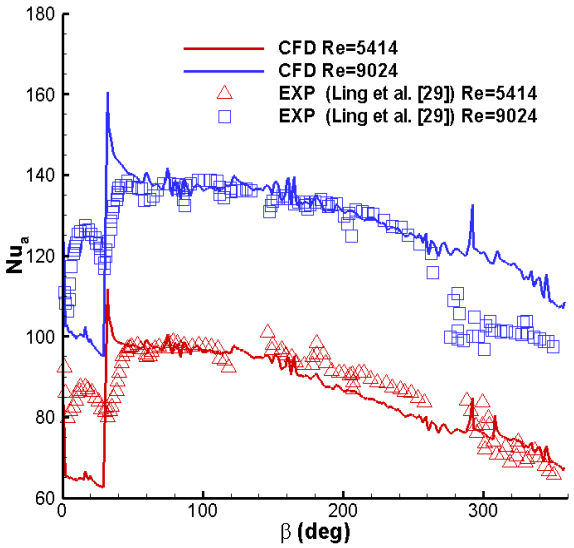

Fig. 16 The variation of axially averaged Nussselt number along the circumference of the swirl chamber with *Re* in geometry (b)

Figure 16 shows the variation of the area weighted axially averaged Nussselt number along the circumference of the swirl chamber by different *Re* in geometry (b). It is also shown that the Nu_a increases with the increase of *Re*. This is because the convective activities are enhanced by the increase of *Re*. The Nu_a decrease gradually with the increase of β when β is larger than 35°. And it is very even along the circumference of the swirl chamber. The numerical results agree well with that of the experimental results by Ling et al. shown in Fig.15.

Hedlund et al. [25] proposed an empirical correlation of globally averaged Nusselt number for swirl cooling in a pipe like geometry (b).

$$\overline{Nu} = 0.63\left(\frac{T_j}{T_w}\right)^{5.7} \mathrm{Re}^{\frac{0.56}{(T_j/T_w)}} \qquad (5)$$

valid for $2{,}000<Re<80{,}000$ and $0.6<T_j/T_w<1.0$.

Figure 17 shows the variation of area weighted globally averaged Nusselt number of the swirl chamber by different *Re* in geometry (a). In the figure, the green line is correlation for fully developed nonswirling turbulent pipe flow predicted by Dittus-Boelter, and the blue line is correlation for swirl turbulent pipe flow predicted by Hedlund et al. It is indicated that the area weighted globally averaged Nusselt number also increases with the increase of *Re*, and the globally averaged Nusselt number of swirl cooling in geometry (a) is always 38% larger than that of the nonswirling turbulent pipe flow, but it is always about 150% lower than that of the swirl cooling in a pipe with two inlet ducts.

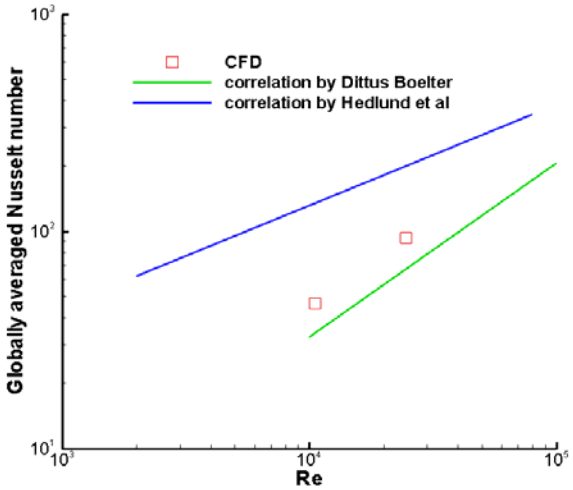

Fig. 17 The variation of globally averaged Nusselt number of the swirl chamber with *Re* in geometry (a)

Figure 18 presents the variation of area weighted globally averaged Nusselt number of the swirl chamber by different *Re* in geometry (b). The area weighted globally averaged Nusselt number also increases with the increase of *Re*, and an excellent agreement is observed with the numerical results of this study and the experimental results by Ling et al. And the gradient of the present study is larger than the correlation got by Hedlund et al. This may be caused by that T_w defined by Hedlund et al. [25] is not the same with its defined in the present study and Ling et al. [29]. The wall condition in the experimental of Hedlund et al. is constant wall heat flux, and the T_w was measured at the section of the

swirl chamber farthest downstream. But the wall condition in the present study and in the study of Ling et al. is constant temperature, which is defined as T_w. The globally averaged Nusselt number of swirl cooling in geometry (b) is about three times of the nonswirling turbulent pipe flow.

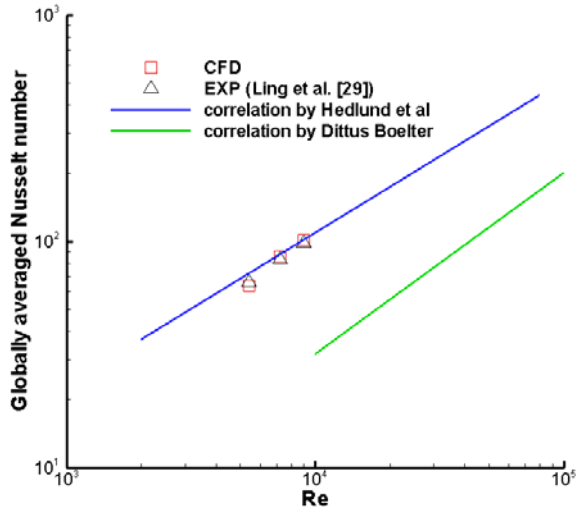

Fig. 18 The variation of globally averaged Nusselt number of the swirl chamber with *Re* in geometry (b)

Effect of inlet to wall temperature ratio

Figure 19 shows the variation of the area weighted circumferentially averaged Nusselt number along the axis of the swirl chamber by different T_j/T_w in geometry (b). It indicates that all along the swirl chamber, for centrifugal forces from helical fluid motion force cooler, denser air moves towards the warmer swirl chamber wall, Nu_c increases with the decrease in T_j/T_w. And with the decrease of T_j/T_w, the increasing amount of Nu_c at each location decrease.

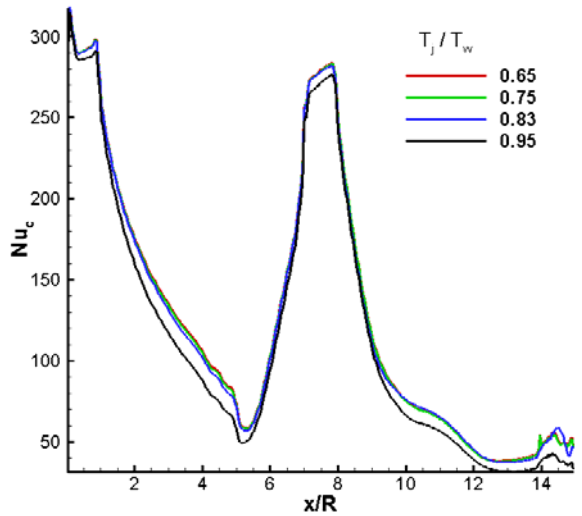

Fig. 19 The variation of circumferentially averaged Nussselt number along the axis of the swirl chamber with T_j/T_w in geometry (b)

Figure 20 shows the variation of the area weighted axially averaged Nussselt number along the circumference of the swirl chamber by different T_j/T_w in geometry (b). The air near the swirl chamber surface is warmer, while the air from the core region of the swirl chamber is cooler and denser. With the decrease of T_j/T_w, the mixing and the replacement of the warmer air and the cooler air enhanced, which lead the Nu_a increases at each value of β. And with the decrease of T_j/T_w, the increasing amount of the Nu_a at each β decrease.

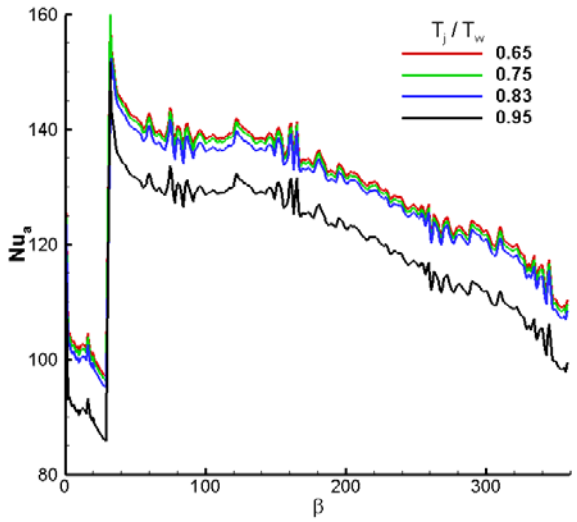

Fig. 20 The variation of axially averaged Nussselt number along the circumference of the swirl chamber with T_j/T_w in geometry (b)

CONCLUSIONS

A numerical simulation has been performed to study the flow and heat transfer of swirl cooling on model of turbine blade leading edge. The influence of impinging fluid Reynolds number and temperature ratio have been analyzed, respectively. Four different turbulence models are validated, and the results show that the SST κ-ω model is the best one of the four tried for solution both of the flow field and heat transfer in the present problem.

The numerical results show that the globally area weighted average Nusselt number of the swirl chamber surface increases with the increase of *Re* and the jet nozzle number. The swirl pipe with two rectangular tangential inlets in this investigation could get a heat transfer enhancement of about three times to that of the nonswirling pipe, while the swirl pipe with one tangential inlet in this investigation could get a heat transfer coefficient 38% higher than that of the nonswirling pipe.

The Nu_c and Nu_a increase with the increase of *Re* and the decrease of T_j/T_w. Each inlet causes a peak of Nu_c. But with the decrease of T_j/T_w, the increasing amount of the Nu_c and Nu_a at each location of the swirl chamber decrease. Furthermore, the Nu_a is very even along the circumference of the swirl chamber.

The decay of the swirl number isn't affected by the *Re*. It only decays along the axis of the swirl chamber and is affected by the rectangular jet.

ACKNOWLEDGEMENT

The authors are grateful for this work supported by China National Basic Research Program (973 Program) Project No.2007CB210107.

REFERENCES

[1] Kreith, F., and Margolis, D., 1959, "Heat Transfer and Friction in Turbulent Vortex Flow," Appl. Sci. Res., Vol.8:457-473.

[2] Kreith, F., and Sonju, O. K., 1965, "The Decay of a Turbulent Swirl in a Pipe," Journal of Fluid Mechanics, Vol.22:257-271.

[3] Nissan, A. H., and Bresan, V. P., 1961, "Swirling Flow in Cylinders," A. I. Ch. E. J., Vol.7:543-547.

[4] Blum, H. A., and Oliver, L. R., 1966, "Heat Transfer in a Decaying Vortex System," ASME Paper GT1966-WA/HT-62.

[5] Migay, V. K., and Golubev, L. K., 1970, "Friction and Heat Transfer in Turbulent Swirl Flow with a Variable Swirl Generator in a Pipe," Heat Transfer-Soviet Research, Vol.3:62-66.

[6] Algigeri, A. H., Bhardwaj, R. K., and Rao, Y. V. N., 1987, "Prediction of the Decay Process in Turbulent Swirl Flow," Proceedings of Institution of Mechanical Engineers, Vol.201:279-283.

[7] Kitoh, O., 1991, "Experimental Study of Turbulent Swirling Flow in a Straight Pipe," J. Fluid Mech., Vol.225: 445-479.

[8] Guo, Z., and Dhir, V. K., 1987, "Effect of Injection Induced Swirl Flow on Single and Two-phase Heat Transfer," ASME HTD. Vol.81:77-84.

[9] Dhir, V. K., and Chang, F., 1992, "Heat Transfer Enhancement Using Tangential Injection," ASHRAE Trans., Vol.98:383-390.

[10] Chang, F., and Dhir, V. K., 1994, "Turbulent Flow Field in Tangentially Injected Swirl Flows in Tubes," International Journal of Heat and Fluid Flow, Vol.15: 346-356.

[11] Chang, F., and Dhir, V. K., 1995, "Mechanisms of Heat Transfer Enhancement and Slow Decay of Swirl in Tubes Using Tangential Injection," Int. J. Heat and Fluid Flow, Vol.16:78-87.

[12] Kumar, R., and Conover, T., 1993, "Flow Visualization Studies of a Swirling Flow in a Cylinder," Experimental Thermal and Fluid Science, Vol.7: 254-262.

[13] Li, H., and Tomita, Y., 1994, "Characteristic of Swirling Flow in a Circular Pipe," ASME Journal of Fluids Engineering, Vol.116: 370-373.

[14] Fitouri, A., Khan, M. K., and Bruun, H. H., 1995, "A Multiposition Hot-Wire Technique for the Study of Swirling Flows in Vortex Chambers," Experimental Thermal and Fluid Science, Vol.10: 142-151.

[15] Chen, J. J., Haynes, B. S., and Fletcher, D. F., 1999, "A Numerical and Experimental Study of Tangentially Injected Swirling Pipe Flows," Second International Conference on CFD in the Minerals and Process Industries, CSIRO, Melbourne, Australia.

[16] Gomez, L., Mohan, R., and Shoham, O., 2004, "Swirling Gas-Liquid Two-Phase Flow—Experiment and Modeling Part 1: Swirling Flow Field," ASME Journal of Fluids Engineering, Vol.126: 935-942.

[17] Gül, H., 2006, "Enhancement of Heat Transfer in a Circular Tube With Tangential Swirl Generators," Experimental Heat Transfer, Vol.19: 81-93.

[18] Guo, H. F., Chen, Z. Y., and Yu, C. W., 2009, "Simulation of the Effect of Geometric Parameters on Tangentially Injected Swirling Pipe Airflow," Computers & Fluids, Vol.38: 1917-1924.

[19] Hay, N., and West, P. D., 1975, "Heat Transfer in Free Swirling Flow in a pipe," ASME Journal of Heat Transfer, PP411-416.

[20] Glezer, B., Moon, H. K., and O'Connell, T., 1996, "A Novel Technique for the Internal Blade Cooling," ASME Paper 96-GT-181.

[21] Moon, H. K., O'Connell, T., and Glezer, B., 1998, "Heat Transfer Enhancement in a Circular Channel Using Lengthwise Continue Tangential Injection," Proceedings of the 11th International Heat Transfer Congress, Vol.6.

[22] Ligrani, P. M., Hedlund, C. R., Babinchak, B. T., Thambu, R., Moon, H. K., and Glezer, B., 1998, "Flow Phenomena in Swirl Chambers," Experimental in Fluids, Vol.24: 254-264.

[23] Thambu, R., Babinchak, B. T., Ligrani, P. M., Hedlund, C. R., Moon, H. K., and Glezer, B., 1999, "Flow in a Simple Swirl Chamber With and Without Controlled Inlet Forcing," Experiments in Fluids, Vol.26: 347-357.

[24] Hedlund, C. R., Ligrani, P. M., Moon, H. K., and Glezer, B., 1999, "Heat Transfer and Flow Phenomena in a Swirl Chamber Simulating Turbine Blade Internal Cooling," ASME Journal of Turbomachinery, Vol.121: 804-813.

[25] Hedlund, C. R., Ligrani, P. M., Glezer, B., and Moon, H. K., 1999, "Heat Transfer in a Swirl Chamber at Different Temperature Ratios and Reynolds Numbers," International Journal of Heat and Mass Transfer, Vol.42:4081-4091.

[26] Hedlund, C. R., and Ligrani, P. M., 2000, "Local Swirl Chamber Heat Transfer and Flow Structure at Different Reynolds Numbers," ASME Journal of Turbomachinery, Vol.122: 375-385.

[27] Hwang, J. J., and Cheng, C. S., 1999, "Augmented Heat Transfer in a Triangular Duct by Using Multiple Swirling Jets," ASME Journal of Heat Transfer, Vol.121: 683-690.

[28] Hwang, J. J., and Cheng, C. S., 2001, "Impingement Cooling in Triangular Ducts Using an Array of Side-entry Wall Jets," International Journal of Heat and Mass Transfer, Vol.44: 1053-1063.

[29] Ling, J. P. C. W., Ireland, P. T., and Harvey, N. W., 2006, "Measurement of Heat Transfer Coefficient Distributions and Flow Field in a Model of a Turbine Blade Cooling Passage With Tangential Injection," ASME Paper GT2006-90352.